Nanosphere Lithography for the Fabrication of Ultranarrow Graphene Nanoribbons and On-Chip Bandgap Tuning of Graphene

Lei Liu, Yingli Zhang, Wenlong Wang, Changzhi Gu, Xuedong Bai, and Enge Wang**

With the rise of graphene research since 2004, the past few years have witnessed rapid progreess in exploiting graphene as an electronic material that shows great promise for future nanoelectronic devices.[1–3] Particular interest in this regard stems from the remarkable electronic properties of graphene, ranging from the extremely high mobility to the tunable carrier type and density.[1,2] However, the fact that graphene is a zero-bandgap semimetal poses a major problem for its practical applications in making high-performance field-effect transistors (FETs).[2,3] As to how an energy gap can be induced in graphene, a known paradigm is to fabricate 1D ultranarrow graphene nanoribbons (GNRs) in which the lateral confinement of charge carriers creates an energy gap near the charge neutrality point.[3–14] Experimentally, ultranarrow GNRs were first fabricated by standard electron beam lithography (EBL) patterning in combination with reactive O_2 plasma etching of graphene sheets;[5,6] however EBL is known to be limited by its serial processing nature, low throughput, and high cost. Later on, the chemically derived GNRs produced via a solution processing route were reported as an alternative, but the synthetic yield was quite low.[7] More recently, some other strategies, e.g., the longitudinal unzipping of carbon nanotubes,[8–10] the inorganic nanowire,[11] and diblock copolymer[12–14] templated etching of graphene sheets, have also been proposed and demonstrated. Despite these important advances, an increasing demand for rapid, massively parallel, high-throughput, and low-cost fabrication strategies for ultranarrow GNRs continues to motivate research.

Here, we present an innovative approach for ultranarrow GNRs fabrication by utilizing nanosphere lithography (NSL)[15] in combination with low-power O_2 plasma etching. NSL, a technique that takes advantage of the self-assembled, ordered arrays of latex nanospheres as lithographic masks for deposition of various metal nanostructures, has long been known to be a inherently parallel, high-throughput, and low-cost nanofabrication strategy.[15] However, in general, a perceived limitation of a common NSL process has been that it can only produce a limited range of nanostructure shapes that are determined by the projection of the nanosphere mask interstices onto underlying substrates.[15,16] In this work, when applying NSL nanopatterning for the lithographic etching of graphene sheets, we surprisingly found that it was capable of fabricating a variety of interesting 1D-based nanoribbon structures. It is shown that the non-uniform and anisotropic distribution of plasma ion, as mediated by the NSL masks, provides a subtle reason for the etching formation of nanoribbons. By proper adjustment of the plasma process parameters, a precision control of the nanoribbon widths is achieved in a size regime comparable with the standard EBL approach.[5,6] Remarkably, due to its unusual simplicity, NSL nanopatterning can be directly implemented into the preintegrated graphene electrical devices for achieving "on-chip" fabrication of GNRs. When subjecting the NSL masked graphene devices to stepwise plasma etching, we were able to monitor in situ the temporal evolution of electrical characteristics as a consequence of the continuous shrinkage of GNRs widths. It is on this basis that we demonstrated a viable and practical methodology for the straightforward on-chip bandgap tuning of graphene.

Two kinds of graphene specimens were used in this work: one was mechanically exfoliated graphene flakes and the other was chemically derived graphene sheets obtained through the well-known graphite oxide (GO) route.[17–21] It is known that mechanically exfoliated graphene specimens possess superior crystal and electronic quality, but are constrained by the extremely low yield of the single-layer sheets. Therefore, to fully exploit the capability of the NSL for GNR fabrication we started with the GO-derived, large-area, single-layer graphene sheets for fabrication experiments. Natural flake graphite was first oxidized to produce GO and then exfoliated in aqueous solution to create a stable colloidal dispersion of the individual single-layered GO sheets. After deposition onto SiO_2/Si substrates, the GO sheets were reduced to graphene by exposure to hydrazine vapors at elevated temperature followed by thermal annealing (see Supporting Information for experimental details). **Figure 1**a shows a representative scanning electron microscopy (SEM) image of the GO-derived single-layer graphene sheets with lateral dimensions up to tens of micrometers lying on a SiO_2/Si substrate. For NSL mask preparation, the deposition and packing of polystyrene (PS) nanospheres (with diameter of ≈1 μm, unless otherwise noted) on substrates was accomplished by adopting a method reported previously (see Supporting

L. Liu, Y. L. Zhang, Prof. W. L. Wang, Prof. C. Z. Gu, Prof. X. D. Bai
Beijing National Laboratory for Condensed Matter Physics
Institute of Physics
Chinese Academy of Sciences
Beijing 100190, P. R. China
E-mail: wwl@aphy.iphy.ac.cn
Prof. E. G. Wang
International Center for Quantum Materials
School of Physics
Peking University
Beijing 100871, P. R. China
E-mail: egwang@pku.edu.cn

DOI: 10.1002/adma.201003847

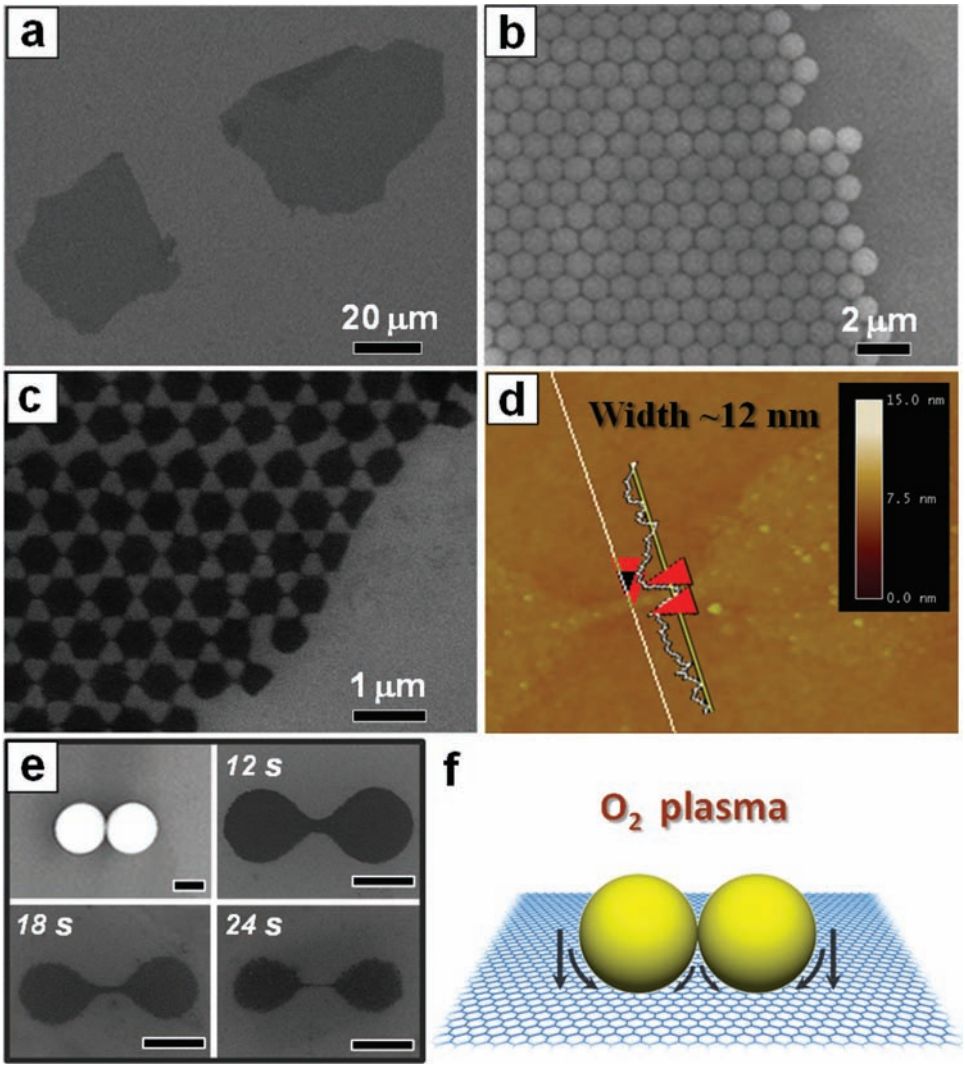

Figure 1. a) SEM image of the chemically derived graphene sheets lying on a SiO_2/Si substrate. b) SEM image showing a domain of the hcp PS nanosphere monolayer that masked the graphene sheets. c) SEM image of the large area, interconnected 2D GNRs network etched through an hcp monolayer NSL mask. Note that the darker areas in the SEM image are GNRs; the image contrast is due to the local potential differences between graphene and the insulating SiO_2 substrate caused by differential charging.[25] d) Tapping mode AFM image of a selected typical nanoribbon with width of ca. 12 nm (measured via line scan profile). e) SEM images showing the temporal evolution of the individual dumbbell-like GNRs etched through the isolated pairs of packed nanospheres (top panel) with etching durations of 12 s, 18 s and 24 s. Scale bars in (e): 500 nm. f) Schematic illustration (not to scale) showing the NSL-defined lithographic etching process of graphene sheets.

Information for details).[22–24] A typical scanning electron microscopy (SEM) image of a domain of the hexagonal close-packed (hcp) nanosphere monolayer is displayed in Figure 1b. The nanospheres masked graphene sheets were subsequently subjected to O_2 plasma etching (Diener Electronic, 40 kHz), after which the masking PS nanospheres were removed by washing with dichloromethane with the aid of mild sonication. Although O_2-based reactive ion etching is a routine procedure for combining with various lithographic techniques in graphene nanofabrication,[5,6,11–14] we must emphasize here that to produce the nanoribbon structures using the present NSL nanopatterning approach, the O_2 plasma etching must be performed at low power such that the etching process of graphene sheets proceeds in a mild and controlled way. Any harsh etching treatment with a high plasma power would otherwise induce etching of the graphene sheets that is too aggressive, leaving behind only the nonbridged, disk-like graphene pads, a similar result to that was recently reported by Cong et al.[16] Typically we chose an optimized plasma processing condition of 30 W at 0.6 mbar with a 10 sccm flow of O_2[26] and varied only the etching time for achieving the desirable etching effects. Figure 1c shows a typical result of the multiply interconnected, ordered 2D network of GNRs etched through a hcp monolayer NSL mask with an etching duration of 21 s. Figure 1d displays the atomic force microscopy (AFM) image of a selected typical nanoribbon by 21 s etching; AFM line scan measurement shows that its lateral diameter is ca. 12 nm. With a longer etching time, even narrower GNRs could be generated, but the problem of over-etching will unavoidably lower the overall yield of GNRs.

To elucidate the formation mechanism for GNRs, the focus is now placed on the temporal evolution of the individual dumbbell-like GNRs that were etched through the isolated pair of packed nanospheres. As depicted in in Figure 1e, with time elapsed, the dumbbell-like GNRs take shape gradually as a consequence of the continuous increase in the aspect ratio of the bridging ribbons along with the gradual size shrinkage of the two side pads. Apparently, the formation of the 1D nanoribbons beneath the nanosphere masks involves a subtle anisotropic etching process that has been related to the non-uniform and anisotropic distribution of the plasma ion flux deflected into the interspacing of the masking nanospheres, as illustrated in Figure 1f. The anisotropy and nanofeature selectivity of the NSL-mediated ion etching process is not a new observation here. In fact, a few previous numerical simulation and experimental studies of NSL have shown such an effect.[27–29] Nevertheless, we note that it is only when the NLS nanopatterning is applied for lithographic etching of the graphene sheets that this anisotropic effect becomes so pronounced that it can eventually lead to the formation of the highly anisotropic, 1D-based nanoribbon structural motifs. It seems likely that the intrinsic anisotropic chemical reactivity of graphene towards the low-temperature and low-power reactive plasma etching also plays a synergistic role in the anisotropic etching process.[30–32]

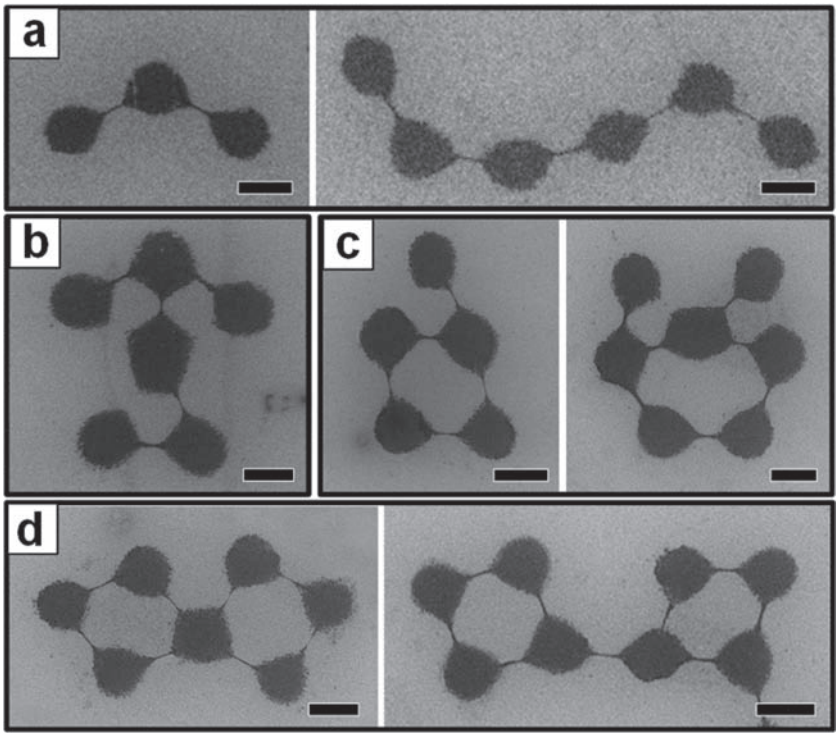

Figure 2. SEM images showing some typical examples of the complex GNRs architectures, including chains (a), branches (b), circular rings (c), and connected rings (d). Scale bars: 500 nm.

Apart from the large-area interconnected networks and the individually addressable dumbbell-like GNRs, we also fabricated a variety of complex architectures with an in-between number of GNRs. This was accomplished by deliberately lowering the nanosphere coverage so as to obtain random masks consisting of sparely distributed, random aggregates of nanospheres (Figure S3, Supporting Information). A few typical examples of the complex GNRs architectures, including the connected GNRs chains, branches, circular rings, and the more exotic connected GNRs rings, are shown in **Figure 2.** The ability to produce not only large-area ordered GNRs networks but also the complex GNRs architectures implies the high versatility of present NSL-based fabrication approach. Importantly, these results further inspired us with a tantalizing possibility: if we can rationally assemble the desired number of nanospheres into uniform aggregates with a well-defined packing geometry, then it would be feasible to rationally control the geometrical structure of the fabricated GNRs architectures. Due to recent advances in spherical colloid assembly research, a physical templating technique is now available for the directed self-assembly of nanospheres into well-defined aggregates at designated regions on solid surfaces.[33,34] For instance, with the use of photolithography patterned relief structures as templates, Xia and co-workers presented an elegant way to assemble spherical colloids into ordered polygonal or polyhedral clusters, linear or zigzag chains, and circular rings.[33] Here, as a preliminary demonstration **Figure 3**a,c shows the assembled nanosphere pentagons and linear chains

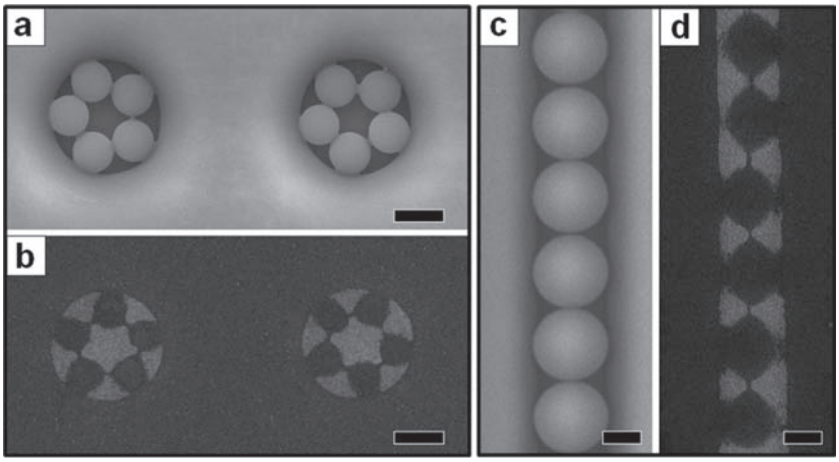

Figure 3. a,c) SEM images showing the well-defined nanosphere pentagons and linear chains formed from ≈1 μm PS nanospheres in the ≈3 μm cylindrical holes of the photoresist and 2 μm spheres in photoresist trenches with ≈2 μm width. b,d) SEM images of the pentagonal ring and linear chain architectures of connected GNRs, etched through the corresponding nanosphere masks. Scale bars: 1 μm.

obtained by the template-directed assembly against the photolithographically patterned cylindrical holes and trenches, respectively. With these well-defined nanosphere aggregates as lithographic etching mask, we fabricated the expected regular pentagonal rings and linear chains of connected GNRs at the designed locations on SiO_2/Si substrates (Figure 3b,d).

As compared to the existing methodologies developed for GNRs fabrication, a key advantage of the present NSL nanopatterining approach is the unusual simplicity and ease of the entire fabrication process. On a practical level, this advantage allows us to directly apply this fabrication approach to graphene sheets that were integrated into electrical devices, such that we were able to achieve the straightforward on-chip bandgap tunning of graphene, as schematically illustrated in **Figure 4**a. For performing the electrical transport studies, we used specimens of the mechanically exfoliated graphene flakes, which are known to possess a superior electronic quality to the GO-derived graphene sheets. Graphene flakes were prepared by micromechanical cleavage from bulk highly ordered pyrolytic graphite (HOPG) and deposited onto a heavily p-doped Si substrate with a 300-nm SiO_2 layer with prefabricated alignment marks. Optical microscopy was first used to identify and locate the single-layer graphene sheets. To further verify their single-layer character, AFM and Raman spectroscopy (the single-layer sheets exhibit a single Lorentzian shape of the G' peak[35]) characterization were also used. The source/drain electrodes were then defined by EBL on the single-layer graphene sheets that were previously located. 20 nm of Pd was then deposited for electrodes by electron beam evaporation, followed by annealing of the devices in Ar at 300 °C for 15 min. Figure 4b shows the AFM image of one of the targeted single-layer graphene FET device that was subjected to NSL masking and a subsequent plasma etching sequence.[36]

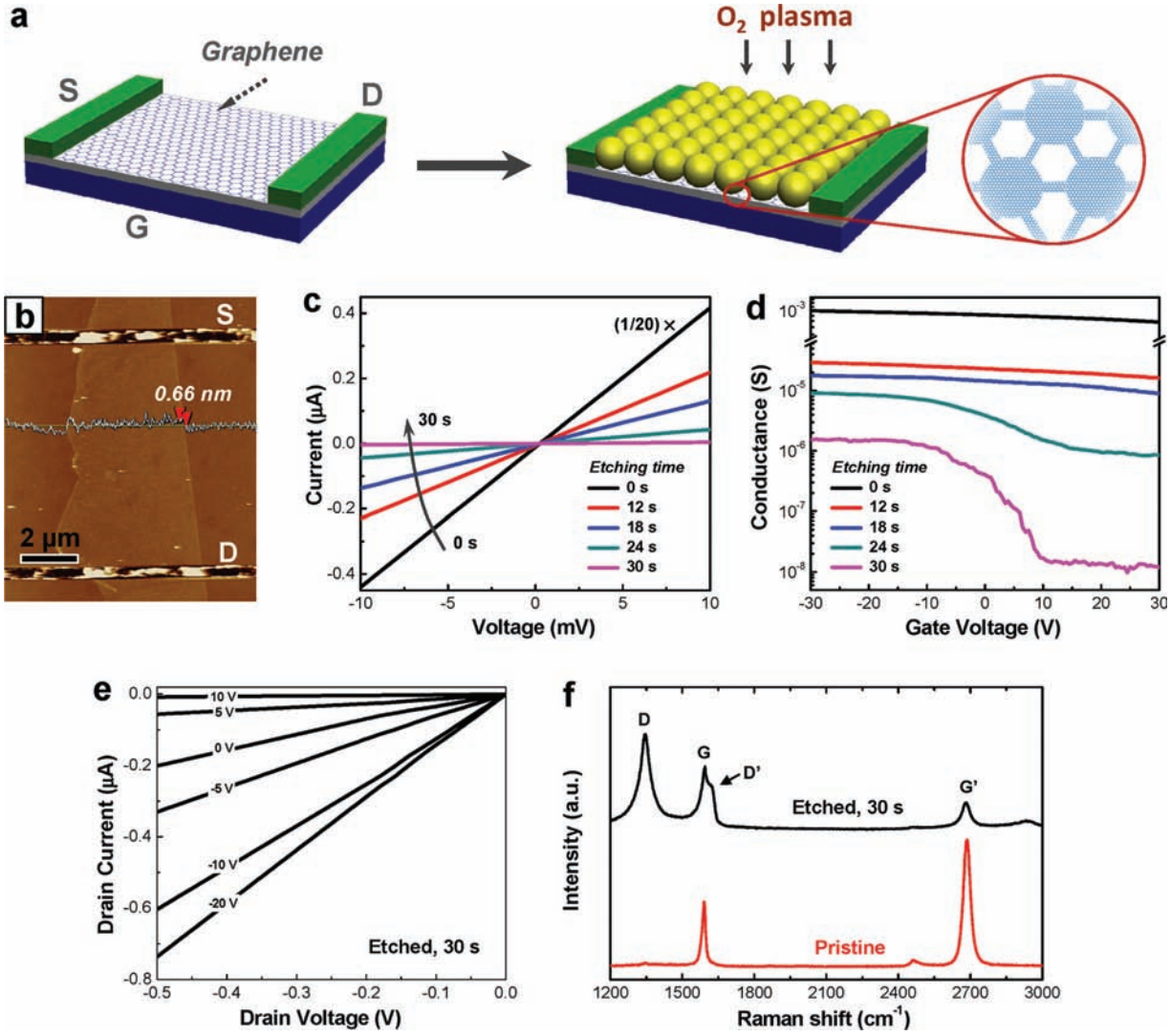

Figure 4. a) Schematic illustration of the on-chip bandgap tuning of graphene through NSL nanopatterning and subsequent O_2-plasma etching. b) AFM image of a typical FET device based on the mechanically cleaved single-layer graphene sheet. c) Evolution of the device current–voltage (I_{ds}–V_{ds}) characteristics for different etching times (12 s, 18 s, 24 s, and 30 s). d) Evolution of the gate-voltage (V_g)-dependent electrical conductance of the same device upon etching. e) I_{ds}–V_{ds} curves recorded under various V_g for the device after 30 s etching. f) Micro-Raman spectra of the pristine graphene sheet and the resultant GNRs network produced by 30 s of etching. The spectra were collected at room temperature using 532-nm laser excitation.

The electrical transport properties of the device were monitored with respect to the plasma exposure time at room temperature. Due to their insulating nature, the presence of the masking PS nanospheres does not affect electrical measurements.

As can be clearly seen from the evolution of the current–voltage data displayed in Figure 4c, with a 12 s plasma exposure of the NSL-masked graphene device, the conductance decreased significantly, while during the remaining etching (18 s to 30 s), the conductance drop become much slower. This fact implies that the line-of-sight etching stage of the graphene sheet occurred mainly within the first 12 s and the lateral etching process started to become dominating within the next etching duration. In Figure 4d, we display the evolution of the transfer characteristics of the same tested device. Prior to plasma etching, the pristine graphene sheet showed little conductance modulation for the entire range of applied gate fields. At the early stage of plasma exposure from 12 to 18 s, a slightly higher on–off ratio was observed, while as the etching time increased to 24 s the device started to exhibit a clear p-type field-effect with the on–off ratio around 10. This indicates that a small portion of the constitute nanoribbons are thin enough that a finite energy gap is opened in them due to lateral confinement. With a further elongated etching time of 30 s, more of the constituent nanoribbons became progressively thinner and the resultant GNRs networks showed more distinct field-effect characteristics (Figure 4d,e). The on–off ratio was enhanced up to ≈90, which is close to the highest achievable on–off ratio of the recently reported graphene nanomesh devices.[11–13] Although an etching time even longer than 30 s is expected to further reduce the average ribbon width, it was found that the problem of partial breakage of the GNRs electrical pathways as induced by over-etching would dramatically sacrifice the on-state conductivity of the GNRs devices.

In Figure 4f, a comparison of the Raman spectrum of the pristine graphene sheet and that of the resultant GNRs network by 30 s etching is shown. Raman spectra were collected over a range from 1200 to 3000 cm^{-1}, and the main differences found in the spectrum of the etched GNRs network is the rise of an additional strong D-band at ≈1345 cm^{-1} and a weak D'-band at ≈1620 cm^{-1}, along with the distinctly reduced ratio of integrated intensity of the G' bands (located at 2685 cm^{-1}) compared to that of the G band (located at 1590 cm^{-1}). These Raman features are due to the presence of irregular edge disorders and oxidized dangling bonds.[35,37] According to current understanding, these edge states will profoundly affect the electronic structures of GNRs.[12–14,38,39] It is assumed that the observed conductance modulations and bandgap opening for GNRs in our experiments may not be solely attributed to the lateral confinement of charge carriers resulting from width narrowing, but rather to a combination of the lateral quantum confinement and the edge disorder effects, as also proposed for the recently reported graphene nanomesh structures.[12] The roles that these factors play in determining the conduction gap of GNRs is still a question that remains open for future theoretical and experimental studies. In the present work, although the NSL-mediated etching formation of GNRs involved a subtle anisotropic etching process, it appears that the as-etched nanoribbons have no crystallographically defined armchair or zigzag type edges.[30–32] Nevertheless, it is possible that, instead of O_2, reactive plasma etching with other weaker oxidizers, such as water vapor and carbon dioxide, may lead to crystallographic selectivity of the NSL-mediated etching process. Follow-up studies are now underway along these lines.

In conclusion, using a combination of NSL and low-power O_2 plasma etching, we demonstrated the rapid and high-throughput fabrication of ultranarrow GNRs. This innovative approach shows the high capability and versatility for creation of the large-area, ordered GNR networks as well as a range of interesting complex GNR architectures including chains, branches, circular rings, and connected rings. By further combining NSL with photolithography patterning, we were able to simultaneously control both the shape and location of the GNR architectures. Room-temperature electrical transport studies verified that NSL nanopatterning could provide a viable and practical methodology for the straightforward on-chip bandgap tuning of graphene. In light of the inherently parallel nature and low-cost of the NSL technique, we expect that the present GNR fabrication approach may open a possible new avenue for the development of graphene-based nanoeletronics.

Supporting Information

Supporting Information is available from the Wiley Online Library or from the author.

Acknowledgements

We acknowledge financial support from the NSF (Grants 50702074 and 20973195) and MOST (Grants 2009DFA01290, 2007CB936203, and 2007AA03Z353) of China.

Received: October 18, 2010
Revised: December 2, 2010
Published online: January 25, 2011

[1] K. S. Novoselov, A. K. Geim, S. V. Morozov, D. Jiang, Y. Zhang, S. V. Dubonos, I. V. Grigorieva, A. A. Firsov, *Science* **2004**, *306*, 666.
[2] K. S. Novoselov, A. K. Geim, *Nat. Mater.* **2007**, *6*, 183.
[3] A. Cresti, N. Nemec, B. Biel, G. Niebler, F. Triozon, G. Cuniberti, S. Roche, *Nano Res.* **2008**, *1*, 36.
[4] Y. W. Son, M. L. Cohen, S. G. Louie, *Phys. Rev. Lett.* **2006**, *97*, 216803.
[5] M. Y. Han, B. Ozyilmaz, Y. B. Zhang, P. Kim, *Phys. Rev. Lett.* **2007**, *98*, 206805.
[6] Z. H. Chen, Y. M. Lin, M. J. Rooks, P. Avouris, *Physica E* **2007**, *40*, 228.
[7] X. L. Li, X. R. Wang, L. Zhang, S. W. Lee, H. J. Dai, *Science* **2008**, *319*, 1229.
[8] D. V. Kosynkin, A. L. Higginbotham, A. Sinitskii, J. R. Lomeda, A. Dimiev, B. K. Price, J. M. Tour, *Nature* **2009**, *458*, 872.
[9] L. Y. Jiao, L. Zhang, X. R. Wang, G. Diankov, H. J. Dai, *Nature* **2009**, *458*, 877.
[10] L. Y. Jiao, X. R. Wang, G. Diankov, H. L. Wang, H. J. Dai, *Nat. Nanotechnol.* **2010**, *5*, 321.
[11] J. W. Bai, X. F. Duan, Y. Huang, *Nano Lett.* **2009**, *9*, 2083.

[12] J. W. Bai, X. Zhong, S. Jiang, Y. Huang, X. F. Duan, *Nat. Nanotechnol.* **2010**, *5*, 190.
[13] M. Kim, N. S. Safron, E. Han, M. S. Arnold, P. Gopalan, *Nano Lett.* **2010**, *10*, 1125.
[14] X. G. Liang, Y. S. Jung, S. W. Wu, A. Ismach, D. L. Olynick, S. Cabrini, J. Bokor, *Nano Lett.* **2010**, *10*, 2454.
[15] a) J. C. Hulteen, R. P. Van Duyne, *J. Vac. Sci. Technol. A* **1995**, *13*, 1553; b) X. Y. Zhang, A. V. Whitney, J. Zhao, E. M. Hicks, R. P. Van Duyne, *J. Nanosci. Nanotechnol.* **2006**, *6*, 1920.
[16] C. X. Cong, T. Yu, Z. H. Ni, L. Liu, Z. X. Shen, W. Huang, *J. Phys. Chem. C* **2009**, *113*, 6529.
[17] N. I. Kovtyukhova, P. J. Ollivier, B. R. Martin, T. E. Mallouk, S. A. Chizhik, E. V. Buzaneva, A. D. Gorchinskiy, *Chem. Mater.* **1999**, *11*, 771.
[18] S. Gilje, S. Han, M. Wang, K. L. Wang, R. B. Kaner, *Nano Lett.* **2007**, *7*, 3394.
[19] C. Gomez-Navarro, R. T. Weitz, A. M. Bittner, M. Scolari, A. Mews, M. Burghard, K. Kern, *Nano Lett.* **2007**, *7*, 3499.
[20] V. C. Tung, M. J. Allen, Y. Yang, R. B. Kaner, *Nat. Nanotechnol.* **2009**, *4*, 25.
[21] Z. T. Luo, Y. Lu, L. A. Somers, A. T. C. Johnson, *J. Am. Chem. Soc.* **2009**, *131*, 898.
[22] F. Burmeister, C. Schafle, T. Matthes, M. Bohmisch, J. Boneberg, P. Leiderer, *Langmuir* **1997**, *13*, 2983.
[23] A. Kosiorek, W. Kandulski, H. Glaczynska, M. Giersig, *Small* **2005**, *1*, 439.
[24] J. Rybczynski, D. Banerjee, A. Kosiorek, M. Giersig, Z. F. Ren, *Nano Lett.* **2004**, *4*, 2037.
[25] a) T. Brintlinger, Y. F. Chen, T. Durkop, E. Cobas, M. S. Fuhrer, J. D. Barry, J. Melngailis, *Appl. Phys. Lett.* **2002**, *81*, 2454; b) A. Vijayaraghavan, S. Blatt, C. Marquardt, S. Dehm, R. Wahi, F. Hennrich, R. Krupke, *Nano Res.* **2008**, *1*, 321.
[26] An even lower plasma power than 30 W was found to lead to unstable and irreproducible plasmas, for our current etching instrument.
[27] L. Q. Yuan, X. X. Zhong, K. Ostrikov, *Nanotechnology* **2008**, *19*, 155304.
[28] A. Kosiorek, W. Kandulski, P. Chudzinski, K. Kempa, M. Giersig, *Nano Lett.* **2004**, *4*, 1359.
[29] X. X. Zhang, D. F. Liu, L. H. Zhang, W. L. Li, M. Gao, W. J. Ma, Y. Ren, Q. S. Zeng, Z. Q. Niu, W. Y. Zhou, S. S. Xie, *J. Mater. Chem.* **2009**, *19*, 962.
[30] L. R. Radovic, B. Bockrath, *J. Am. Chem. Soc.* **2005**, *127*, 5917.
[31] D. E. Jiang, B. G. Sumpter, S. Dai, *J. Chem. Phys.* **2007**, *126*, 134701.
[32] P. Nemes-Incze, G. Magda, K. Kamaras, L. P. Biro, *Nano Res.* **2010**, *3*, 110.
[33] Y. D. Yin, Y. Lu, B. Gates, Y. N. Xia, *J. Am. Chem. Soc.* **2001**, *123*, 8718.
[34] Y. D. Yin, Y. N. Xia, *J. Am. Chem. Soc.* **2003**, *125*, 2048.
[35] A. C. Ferrari, J. C. Meyer, V. Scardaci, C. Casiraghi, M. Lazzeri, F. Mauri, S. Piscanec, D. Jiang, K. S. Novoselov, S. Roth, A. K. Geim, *Phys. Rev. Lett.* **2006**, *97*, 187401.
[36] Note that as compared to the chemically derived graphene sheets, the mechanically cleaved graphene flakes are more resistant to plasma etching and thus necessitated a longer etching time than that for chemically derived graphene specimens.
[37] A. K. Gupta, T. J. Russin, H. R. Gutierrez, P. C. Eklund, *ACS Nano* **2009**, *3*, 45.
[38] M. Evaldsson, I. V. Zozoulenko, H. Y. Xu, T. Heinzel, *Phys. Rev. B* **2008**, *78*, 161407.
[39] F. Sols, F. Guinea, A. H. Castro Neto, *Phys. Rev. Lett.* **2007**, *99*, 166803.